Science

Mesoscale Modeling of the Circulation in the Gale Crater Region: An Investigation into the Complex Forcing of Convective Boundary Layer Depths

Daniel Tyler Jr.[1] and Jeffrey R. Barnes[1]

[1]College of Earth, Ocean and Atmospheric Sciences, Oregon State University, Corvallis, OR, 97331, USA, dtyler@coas.oregonstate.edu

Abstract

Background: Atmospheric mesoscale modeling [performed in support of Mars Science Laboratory Entry Descent and Landing (MSL EDL) at L_s=151°] is used in a high-resolution investigation of the complex circulation in and near Gale Crater. Model results show that afternoon Convective Boundary Layer depths are dramatically suppressed over the northern crater floor. For nearly the same locations, excursions from the expected surface pressure cycle are large, with daytime lows and nighttime highs that exceed the expected values by ~1.5%.

Method: The 20-sol meteorological mean diurnal cycle is constructed for the innermost 4 km nest of the OSU Mars Mesoscale Model (OSU MMM). In examining the mean diurnal cycle, important forcings are identified. Numerous slices of winds and potential temperature are used to describe the circulation. Additionally, a diagnostic surface pressure field (based on the relationship between surface pressure and topography) is constructed to provide a dynamically unmodified surface pressure field. The difference between the actual surface pressure field and the diagnostic field is examined, identifying the locations and amplitudes of surface pressure excursions. The relationship between surface pressure excursions and dynamics is investigated.

Conclusion: This study reveals that intra-scale interactions (between the larger-scale slope flows across the dichotomy boundary and those caused by Mt. Sharp and the rim walls of Gale Crater) excite smaller-scale circulations that modify the vertical temperature structure most significantly over the northern crater floor. Analysis shows that these circulations are generally mass-conserving, producing subsidence during the day and upwelling at night, and are largely responsible for modifying the temperature of a deep (~3 km) column of air. The modified vertical temperature profile is seen to correspond better with elevation above the mean regional topography than elevation above local topography (the "typical" case for Mars). Convective Boundary Layer (CBL) depths and surface pressures are significantly affected in response to the modified air temperature. In a constructive interaction between dichotomy boundary and crater slope flows, hydraulic jumps are seen to form late at night in craters near the base of the southern rim walls. In Gale Crater, a vigorous hydraulic jump forms near the southwest rim, and persists through early morning with wind speeds reaching ~35 m/s. With nearly constant periods of heating and cooling near the equator throughout the year, an important role for aeolian processes in Gale and other craters along the dichotomy boundary is likely.

Introduction

In support of Mars Science Laboratory, most specifically getting Curiosity safely onto the surface of Mars, a great deal of mesoscale modeling was performed to characterize the late-afternoon atmosphere and investigate the range of meteorological variability and risk involved in landing at the proposed sites. Vasavada et al. (2012) provide a good overview of this modeling. In this paper we examine the full diurnal cycle of the circulation in and near Gale Crater, as simulated by one of the involved models, the Oregon State University Mars Mesoscale Model (the OSU MMM).

Gale Crater is centrally located near the foot of a steep section of the dichotomy boundary. In this region, strong upslope/downslope flows are expected to have a significant effect on the wind regime during both day and night. In a comparison of results from four different mesoscale models that simulated the Gale Crater circulation, Haberle et al. (2012) describe how surface winds inside Gale Crater do not follow the expected larger-scale behavior simulated by the NASA-Ames Global Climate Model (GCM). In the GCM, tidally induced regional pressure gradients and dichotomy boundary slope flows are the primary components of the diurnal forcing. Inside Gale Crater, unresolved by the GCM, surface winds exhibit a very complex diurnal cycle, highlighting the importance of the much smaller-scale slope flows excited by the crater walls and Aeolis Mons (Mt. Sharp). Winds inside the crater appear to be mostly "shielded" from the larger-scale slope flows across the dichotomy boundary, especially so for the lowest elevations in the northern interior where Curiosity landed. In consideration of these vastly different scale slope flow forcings, an analysis of mesoscale model results was undertaken to better understand the circulation.

There are many craters along the dichotomy boundary where the local crater and regional dichotomy boundary slope flows will interact. In this regard Gale is certainly not unique. However, Gale Crater does exhibit a high degree of asymmetry in the meridional direction in two very important factors: albedo and topography. Spatial variability in these surface properties can be very important dynamically. The existence of Mt. Sharp makes Gale Crater even more unique, adding an important dimension to the crater circulation by forcing slope flows at the center of the crater and not just at the rim walls. Since Gale Crater is very near the equator, the Coriolis effect is negligible. This simplifies the force balance and the development of the circulation over the diurnal cycle, although it also means that model dynamics depend more highly on parameterized forcing in the momentum equations. This is a well-known challenge in atmospheric modeling.

Over a very wide range of scales, dramatic topographic relief is a defining aspect of the surface of Mars. Moreover, if we use a very basic scaling of solar flux to surface air density to compare Mars and Earth, the atmospheric response to solar forcing on Mars is ~33 times greater than it is on Earth [air density on Mars is ~75 times less, while the solar flux is on average ~2.3 times less, (1/2.3)/(1/75) ~ 33]. In response, very large amplitudes are observed in the diurnal cycle of ground and near-surface air temperature. The result is that slope flows must be ubiquitous on Mars, and they will exist over a wide range of scales that most certainly have complex interactions. As described by both Tyler et al. (2002) and Rafkin and Michaels (2003), when strong slope flows exist within a closed or semi-closed basin (Valles Marineris is the example used in both), a significant response in the diurnal cycle of surface pressure is expected. And, as described by Spiga et al. (2007), OMEGA observations show that surface pressure inside moderately sized craters can also be affected. For Gale Crater, both local and regional slope flows play a

role in the diurnal meteorological cycle; and, interactions are certain to excite additional circulations.

The OSU MMM predicts very small Convective Boundary Layer (CBL) depths in the interior of Gale Crater, as shown by both Vasavada et al. (2012) and Haberle et al. (2012). Observations from orbit appear to support this result, showing that dust devils are rare or non-existent within Gale Crater (Cantor, 2006; personal communication, Bruce Cantor, 2012). In this paper we explore, and try to explain, the interactions between the regional and crater circulations that are involved in causing the very small CBL depths over the northern floor of Gale Crater. With Curiosity heading towards Mt. Sharp, it is hoped that wind data from REMS (Rover Environmental Monitoring Station) will provide observations that can help validate and/or improve simulations of the complex circulation within Gale Crater.

The OSU MMM and Model Results

The OSU MMM

As described by Vasavada et al. (2012), the Oregon State University Mars Mesoscale Model (the OSU MMM) is one of two mesoscale models used in a comprehensive modeling effort in support of Mars Science Laboratory Entry Descent and Landing (MSL EDL). In this paper, results from simulations performed for MSL with the OSU MMM are examined over the complete diurnal cycle. The results presented in this paper are from "nominal" case runs. The dust prescription for "nominal" case runs is the result of an iterative tuning process, where the NASA-Ames GCM was repeatedly run with small adjustments to the dust prescription. Each adjustment provided a "tuning" towards a better agreement with observed atmospheric temperatures. Starting from TES observations of the total column dust opacity (Smith, 2006), the "nominal" case dust prescription is shown in Fig. 1. The OSU MMM uses the same radiation parameterization as the NASA-Ames GCM (Tyler et al., 2002), so this process also facilitated a "tuning" of the OSU MMM. The NASA-Ames GCM provides initial and boundary conditions for the OSU MMM and is run in seasonal mode for a period of 60 sols. The seasonal cap edges, seasonal cap albedo and emissivity values, and initial atmospheric mass are all prescribed (part of the "tuning" process) to provide the best representation of the observed seasonal climatology. The first 30 sols allow the GCM to "spin up" from a cold start, and the final 30 sols provide initial and boundary conditions for the OSU MMM.

The grid space hierarchy of modeling domains that constitute a run of the OSU MMM is shown in Fig. 2. The OSU MMM is run hydrostatically, with 55 sigma layers in the vertical and the model top at 0.01 Pa. Modeling domains are polar stereographic, with a super-hemispheric mother domain reaching deep into the northern hemisphere. As discussed by Tyler et al. (2002), there are advantages when using this configuration. Moreover, for late southern hemisphere winter on Mars, the strong jet and baroclinic zone are well resolved, and the influence of these structures
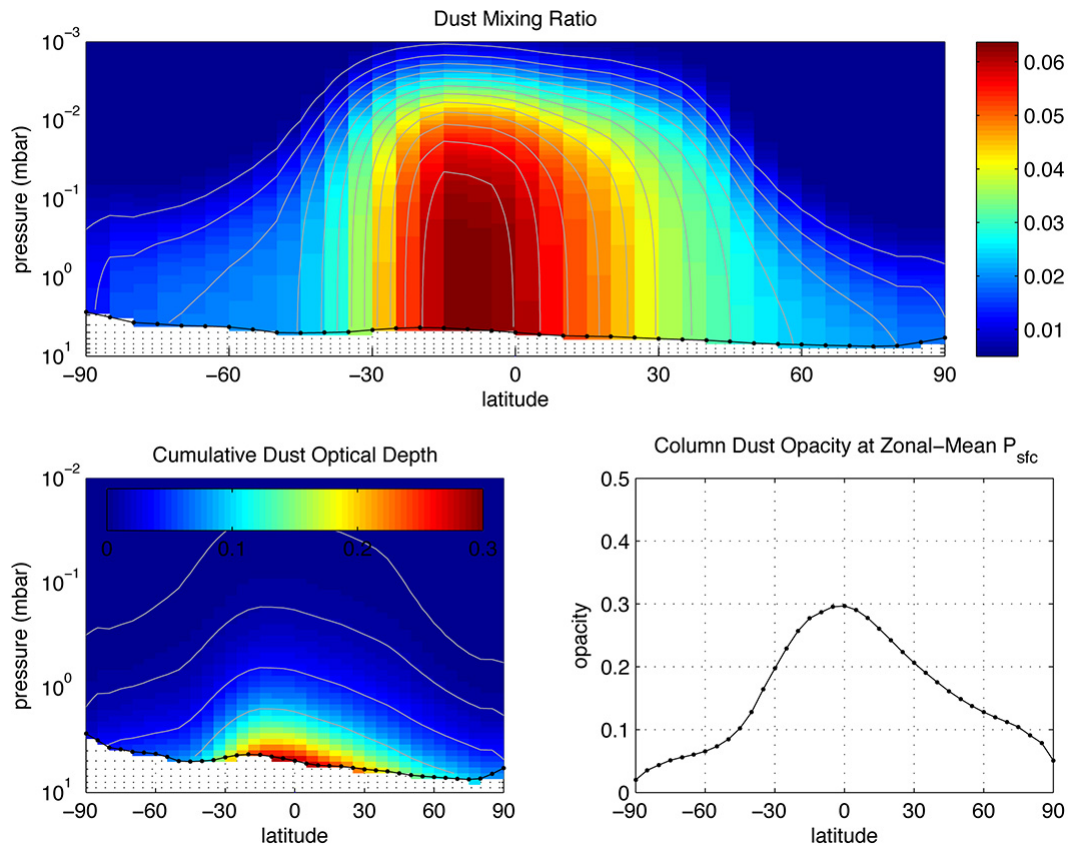
Figure 1. The zonal-mean dust distribution used in the OSU MMM, and the NASA-Ames GCM that provides initial and boundary conditions for the mesoscale model. The total column dust opacity is prescribed at the zonal-mean surface pressure (bottom right) as a function of latitude. In the vertical, the mixing ratio (top) has a Conrath-Nu formulation that depends on latitude (Figure01.jpg).

in low latitudes can be examined to develop variance statistics along and near the storm track (see Vasavada et al., 2012). The model is run for 30 sols, where the final 20 sols (that are used for analysis) are centered in L_s on the actual date of MSL EDL (L_s=151°).

Three levels of nesting are used in a run of the OSU MMM. The upper right subplot of Fig. 2 (the first nest) shows how Gale Crater is centrally located at the foot of a steep section of the dichotomy boundary. In this study, the model output analyzed is from the modeling domain shown in the bottom right subplot of Fig. 2. This third-level nest is 130x130 and has a nominal spatial resolution of 4 km; it is in two-way feedback with the region it shares with the second level nest (its 12 km resolution parent domain). In the vertical, the resolution is very good in the lowest ~10 km; there are 27 model layers below ~10 km and 15 below ~1 km (not shown). The center of the lowest model layer is at ~5 m AGL, the lowest level where winds and air temperature are carried in the simulation. Sufficient resolution in the vertical is required to resolve the winds near the surface that are important in the development of the Convective Boundary Layer, especially in regions of complex topography. The Planetary Boundary Layer (PBL) scheme used in the OSU MMM is the MRF, as described by Hong and Pan (1996).

The scheme is essentially a local-K approach, with the addition of a counter-gradient flux term (nonlocal diffusion) as described by Troen and Mahrt (1986). The PBL scheme is mostly unmodified, although 1) some constants have been modified to allow greater vertical diffusion, 2) the "free atmosphere" level check in the scheme was made appropriate for Mars, and 3) the sponge layer at the model top is deeper, modified in shape and stronger. Collectively these changes appear to have somewhat improved model stability by decreasing "noise" near the top of the model, otherwise leaving the solution unaffected.

Finally, in Fig. 3 the topography and albedo of the 4 km nest are presented in latitude/longitude space instead of grid space. The albedo maps used in the OSU MMM are constructed from the data of Putzig and Mellon (2007). A latitude/longitude orientation is more standard than that of Fig. 2, allows for easier discussion, and will be used from this point forward.

Surface Winds

With slope flows across the dichotomy boundary, and slope flows excited by the steep and smaller-scale topographical features (hills, smaller craters, the rim walls of Gale Crater and Mt. Sharp), the diurnal cycle of surface winds is highly
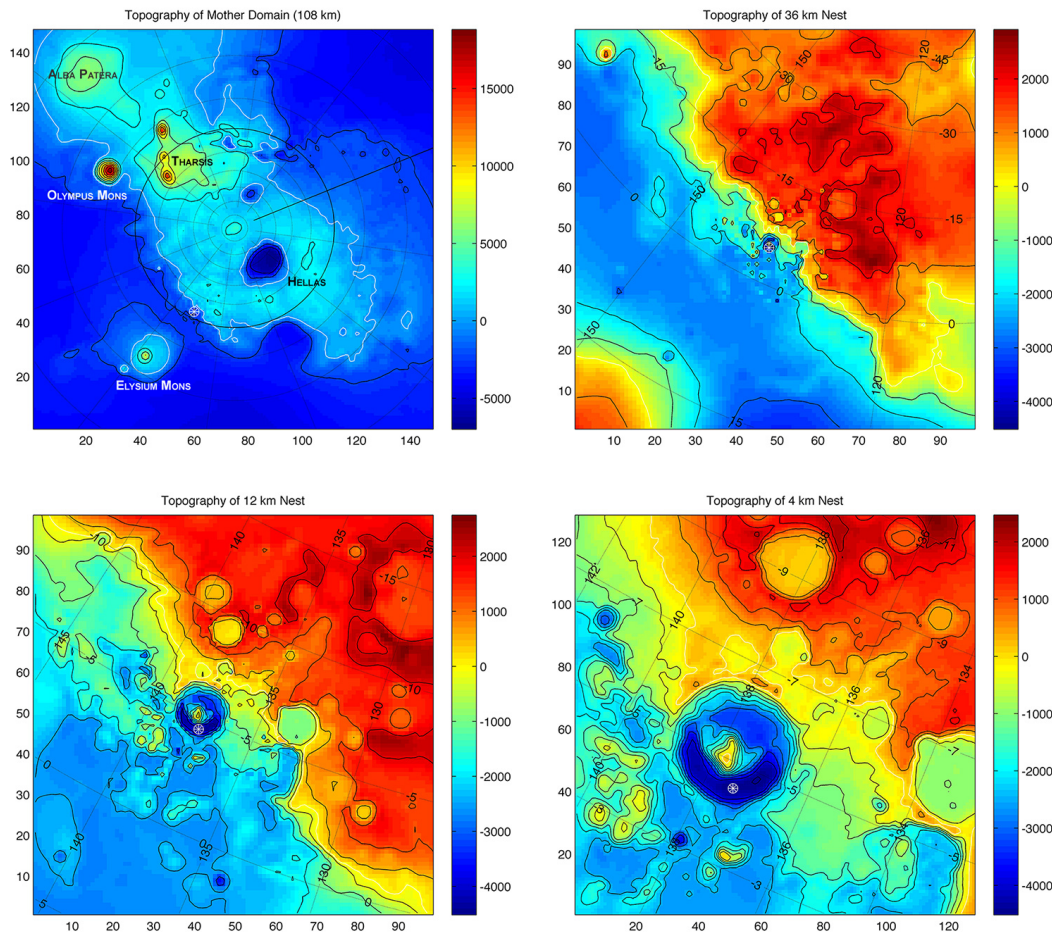
Figure 2. Model topography shows the grid space hierarchy of the OSU MMM modeling domains. In the upper left subplot, with labels to aid spatial orientation, the mother domain is shown (~108 km). GCM boundary conditions are applied at the mother domain boundaries. The South Pole is at the center of the mother domain; the equator is identified with a heavy black circle and other latitudes are shown at 15° intervals. The first nest (~36 km) is shown in the upper right subplot; the bottom left is the second nest (~12 km); the bottom right is the third nest (~4 km). There is a 3x increase in resolution for each nest (lat/lon contours are shown and labeled for each nest). The landing site is marked with a circled white asterisk in each subplot. (Figure02.jpg).

complex in the region of Gale Crater. For the lowest model level in the 4 km nest (~5 m AGL), surface winds at four times of day are shown in Fig. 4 (where wind vectors are drawn at every other grid point). Each vector is a 20-sol mean (an average of 20 wind vectors at one UTC time), where the local true solar time (LTST) is valid at the landing site ellipse center (LTST varies by ~30 min over the range of longitudes). In using the mean diurnal cycle, any transient meteorological excursions are averaged out, which means that features seen in the wind field are true features of the mean diurnal cycle.

At ~0230 LTST, the surface flow is everywhere downslope, into all craters and basins, down all topographical shelves, and outward and downward from the tops of the hills NE of Gale Crater. Maximum wind speeds are ~20 m/s. An interesting acceleration and convergence feature is seen where the flow down the dichotomy boundary enters the west side of the crater. The wind is accelerated by the additional slope flow forcing of the crater rim and the

resulting convergence is enhanced in response to the curvature of the crater rim. At this time of night, a lot of variability is seen in the wind field, and this variability is related to smaller-scale topography.

By ~0830 LTST, the winds inside Gale Crater have turned upslope, while the downslope dichotomy boundary flow appears stronger (especially so in the channel to the west of Gale Crater at a lat/lon location of -4.5°/135.5°E). Since the Sun is now warming the ground, exciting some low-level turbulent mixing, flow down the dichotomy boundary is less modified by smaller-scale topographical features and appears more uniform (with the ground warming, smaller-scale topographical "steering" of the nocturnal drainage rapidly ends). At the SW rim of Gale Crater, the early morning upslope flow is in opposition to the downslope dichotomy boundary flow. The near-surface convergence that results can excite a strong morning updraft. Describing an interaction between the local Gusev Crater circulation and that of the thermal tides, Rafkin and Michaels (2003) have

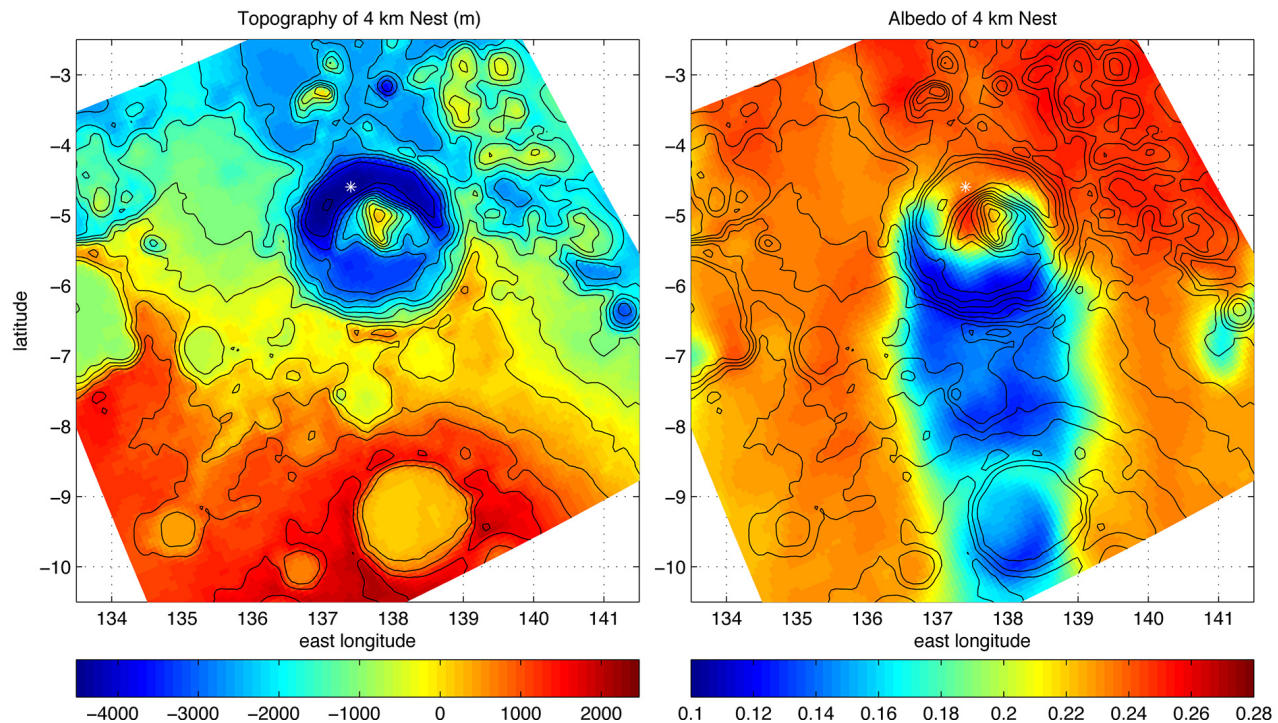Topography of 4 km Nest (m)   Albedo of 4 km Nest

Figure 3. The topography and albedo maps for the 4 km grid-spacing nest are shown in latitude/longitude space. In the maps, topography is contoured at 500 m intervals and the location of the landing ellipse center is identified with a white asterisk. Albedo is derived from the global maps of Putzig and Mellon (2007) (Figure03.jpg).

noted the importance of convergence zones.   At ~0830 LTST, surface insolation is more intense at the SW crater rim due to the slope direction.   When residual downslope dichotomy flow encounters flow that has turned upslope at steeper local topography features, other locations are also seen to exhibit convergence.

By ~1430 LTST the flow is everywhere upslope, and compared to ~0230 LTST this change is dramatic for the hills NE of Gale Crater.   Strong upslope dichotomy boundary flow is seen at the steepest part of the topographical gradient, which produces a widespread region of convergence.   Additionally, a prominent and long (~250 km) convergence zone can be seen to extend from the eastern side of Gale Crater up the dichotomy boundary and into the large crater at a lat/lon location of 9.25°S/138.25°E. This curvilinear zone of convergence produces a similarly shaped feature in the vertical velocity field (~3-5 m/s at ~3-5 km above the surface).   The location of this feature is well correlated with the gradient in the surface albedo (see Fig. 3). Again, these are 20-sol mean winds, so this feature is part of the mean diurnal cycle.   Many smaller convergence zones are evident at this time, and vertical velocities in the model are generally significant above each of them.   Some convergence locations are fixed spatially while others move with time (up the dichotomy boundary).   By ~2030 LTST, the dichotomy boundary flow has begun to transition into a nocturnal drainage mode (as can be seen to the east of Gale Crater).   By this time, however, strong downslope flow is already well established within Gale Crater and on the slopes of Mt. Sharp.

The surface winds, at the four times of day in Fig. 4, show that the phase of the two slope flow forcings (that of the dichotomy boundary and that of the crater rim walls and Mt. Sharp) is not the same. And, at the north rim of Gale Crater, as compared to the south rim, strong slope flow from the dichotomy boundary is never seen. The location of the north rim, not directly on the topographical gradient of the dichotomy boundary (as is the south rim), is important. Mt. Sharp certainly has an important role in the diurnal cycle of upslope and downslope winds within Gale Crater (more discussion later). For the circulation at the north rim, the simple fact that the topography of the crater rim slopes in the opposite direction of the dichotomy boundary is important. In itself this means a phase difference of 180° between the two slope flows. If the dichotomy boundary slope flows reached maximum and minimum strength at the same times as those on the crater rim walls, the superposition of slope flows would always be constructive at the south rim and destructive at the north rim. As Fig. 4 shows, this is not the case. When we consider the phase difference between the two slope flows (not the same for the north and south rims of Gale Crater), the asymmetries in topography and albedo, and the additional crater circulation excited by Mt. Sharp, we can understand why the circulation in and near Gale Crater is so highly complex.

Convective Boundary Layer Depths

Using model potential temperatures, Convective Boundary Layer (CBL) depths are constructed for the OSU MMM. For Gale Crater and the local region, model CBL depths are shown in Fig. 5. Within the period of 1400-1600 LTST,
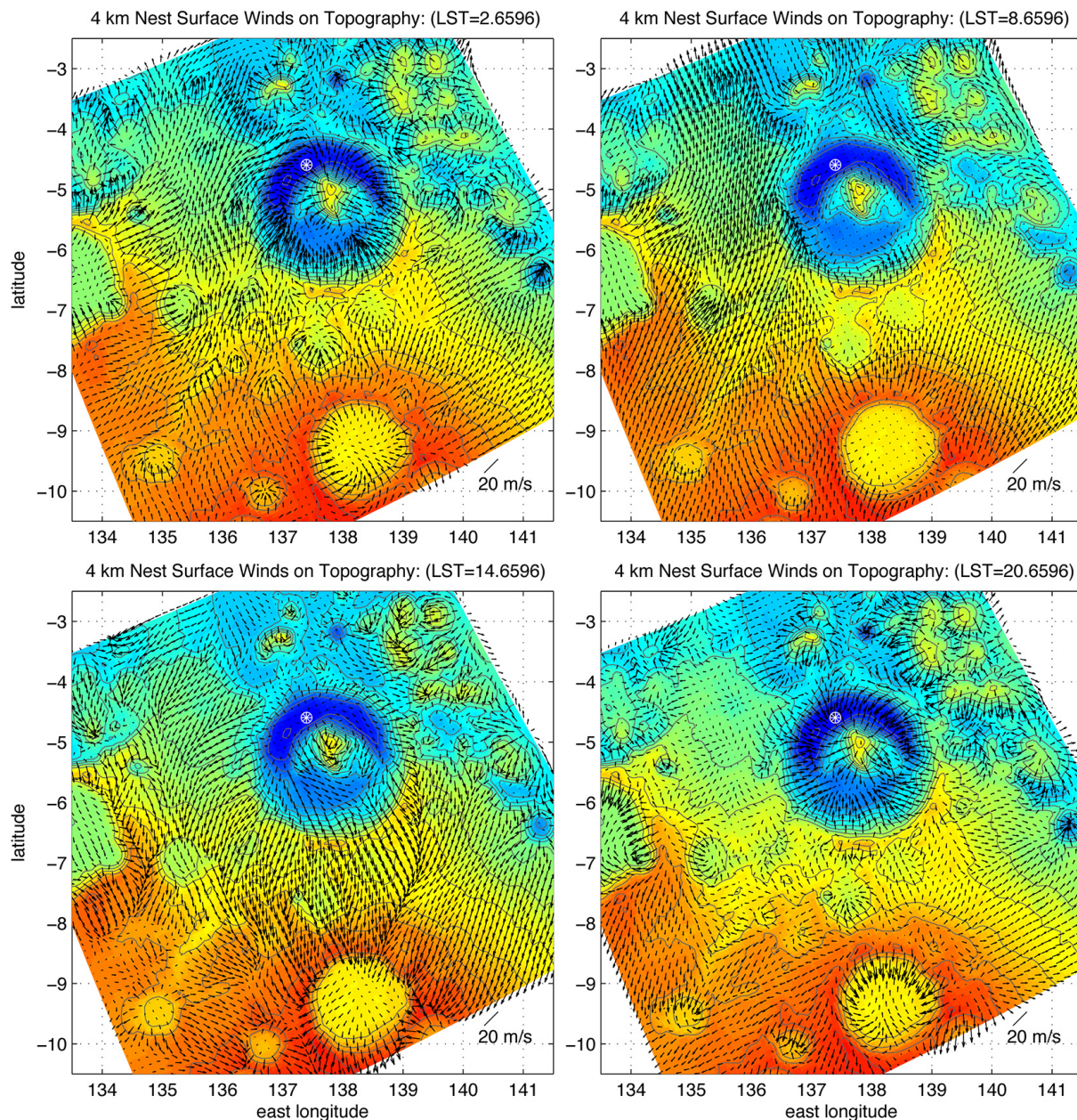
Figure 4. The 4 km nest surface winds (~5 m AGL) are shown at four local times of day at every other grid point (to reduce clutter). The winds are from the 20-sol mean diurnal cycle (time at the landing site ellipse center is shown in the subplot title). Topography is color-shaded and contoured in 500 m intervals. The X and Y axes are longitude and latitude (Figure04.jpg). A GIF animation of the full diurnal cycle at bi-hourly intervals is available (SfcWinds4km.gif).

when the CBL is typically deepest, potential temperature profiles are used to construct the data shown in Fig. 5. The CBL depth of a single profile is determined by comparing the change in potential temperature with height to a small positive numerical threshold value (comparison proceeds upwards from the ground). The height above the ground, where the potential temperature gradient first becomes greater than the threshold value (0.75 K/km was used to construct these data), is taken to be the depth of the CBL at that location and time. Since the potential temperature gradient will always be negative at the ground during this time period, this procedure is robust. Using all depths for a

single location, an average is taken (twenty sols of bi-hourly model output yield sixty CBL depths in the time window). The very small CBL depths seen over the northern floor of Gale Crater were key in motivating this investigation. The sharp horizontal change in CBL depths at the northern rim of Gale Crater must involve smaller-scale dynamics.

The Mars Express radio occultation experiments described by Hinson et al. (2008) provide an excellent example of how the CBL depth generally increases with the elevation of the surface. In Fig. 5, even though the 4 km nest is too small to

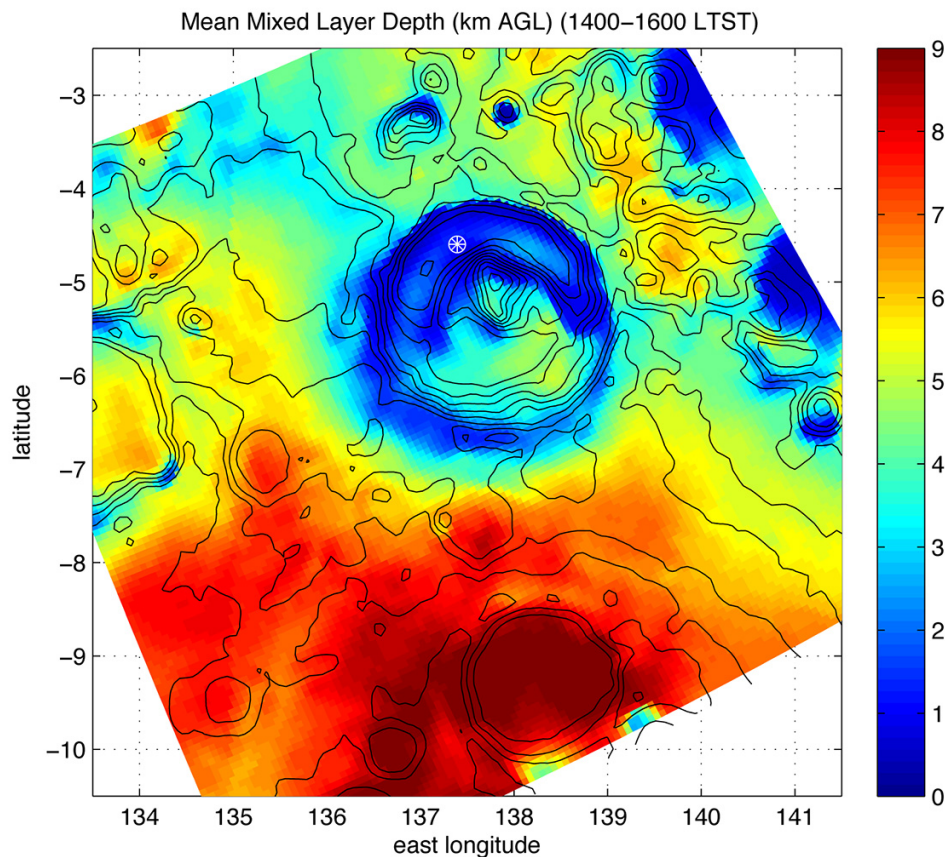Mean Mixed Layer Depth (km AGL) (1400–1600 LTST)

Figure 5. Afternoon mixed layer depths from the OSU MMM are shown for the 4 km nest. The result is 20-sol average of model data in the time window of 1400-1600 LTST at each location. The center of the MSL landing ellipse is shown with a circled white asterisk, and MOLA topography is contoured at intervals of 500 m (Figure05.jpg).

provide wide regional context, we do see that the greatest CBL depths occur higher up the dichotomy boundary to the south. Since there is less atmospheric mass to warm above higher elevation locations, the CBL grows deeper. When the CBL depths in the OSU MMM are examined over a larger region at lower model resolution (not shown), the correlation with surface elevation is quite clear. It is worth pointing out, that while insolation decreases at locations further to the south (albeit by a small amount), CBL depths in Fig. 5 are generally still much deeper over the higher elevations.

In a more critical examination of Fig. 5, we do see many examples of CBL depths that appear to vary independently from the local topography. Not all crater interiors are seen to have smaller CBL depths than those over the higher elevations outside the crater (specifically, at a lat/lon location of 9.25°S/138.25°E, the CBL is larger inside the crater). Additionally, some "hills" are seen to exhibit suppressed CBL depths, while other craters simply exhibit CBL depths that would be expected for the elevation of the local topography (all else being equal). This evidence suggests that local atmospheric dynamics play an important role in determining the depth of the CBL.

Zones of convergence and divergence in the near-surface flow can produce vigorous motion in the vertical. As mentioned above, good spatial correlation is seen between convergence zones in the surface wind field and strong updrafts in the model. Given the propensity for (and strength of) slope flows on Mars, convergence must be a very important dynamical mechanism for exciting updrafts and vertical mixing, two factors that certainly influence the depth of the CBL. In fact, the greatest CBL depth in Fig. 5, seen in the crater at a lat/lon location of 9.25°S/138.25°E, is directly related to the strong convergence zone that moves through the crater in the afternoon (see Fig. 4). It is a theme worth repeating: interaction between vigorous slope flow circulations must exist at a great many scales and locations on Mars. The resulting convergence zones, that may be spatially fixed or not (both types can be seen in Fig. 4), are almost certainly important for the depth of the CBL. Conversely, with divergence in the near-surface wind field there will be subsidence, and depending on the subsidence velocities, the adiabatic warming has the potential to make the atmosphere much more stable, which would inhibit the growth of the CBL.

In Figs. 2a and 2c of Hinson et al. (2008), afternoon temperature profiles from different locations are shown on the same set of axes. A similar figure can be constructed for the Gale Crater region. This is most easily done using output from an *otherwise identical lower resolution run* of the OSU
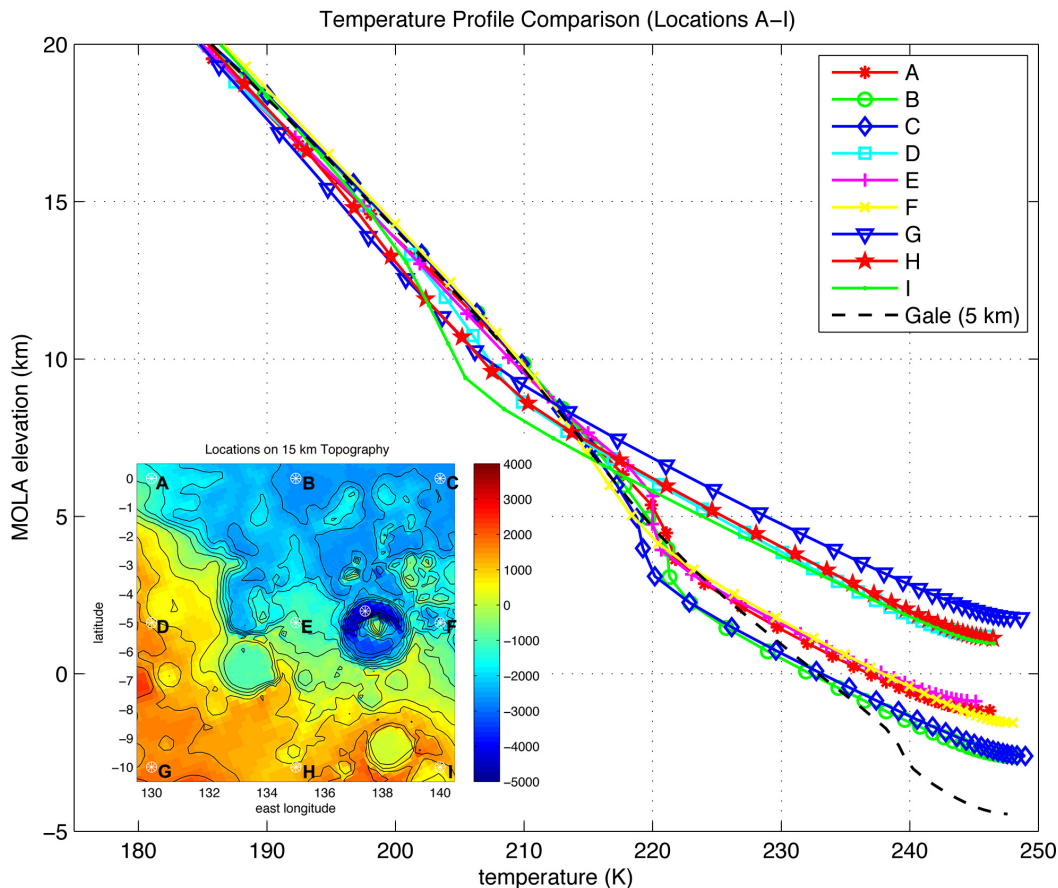
Figure 6. Locations of nine 20-sol mean temperature profiles (1400-1600 LTST) can be seen in the inserted subplot (noted by letters A-I). The nine profiles at these locations are plotted in the figure body. Different colors and markers are used for each profile shown. A marker is plotted at the MOLA elevation of each temperature in the profile. These data are from a run that ***differs only in horizontal resolution*** from the primary run. At the A-I locations, data is from a 15 km nest. For the Gale profile (the black dashed line) the data is from the 5 km is next at the landing site ellipse center (Figure06.jpg).

MMM (with the mother domain at 135 km, and the nests at 45 km, 15 km and 5 km). In this lower resolution run, the 5 km nest still resolves Gale Crater quite well [see Vasavada et al. (2012) for the 5 km analogue of Fig. 5 in this paper], while the 15 km nest provides much broader coverage of the region than the 12 km nest. Using nine locations from the 15 km nest that straddle the dichotomy boundary (and Gale Crater), the 20-sol mean afternoon (1400-1600 LTST) temperature profiles are examined in Fig. 6. To compare the crater interior to the other locations, the ellipse center profile from the 5 km nest is also shown. The location of each profile is identified in the subplot insert, and each is plotted with a different color/marker combination in the body of the plot. The locations A, B, C, E and F are the profiles over lower elevation ground, and they all have shallower CBL depths of ~4 km; the locations D, G, H and I are the profiles over higher elevation ground, and they all have deeper CBL depths of ~7 km.

When comparing Fig. 6 with Figs. 2a and 2c of Hinson et al. (2008), we see that the model temperature profiles provide a good representation of the temperature versus elevation

relationships observed by Radio Science. In Fig. 6, the difference between the surface elevations of locations C and G is similar to that in Figs. 2a and 2c of Hinson et al. (2008). In the model temperature profiles, the horizontal difference in air temperature (~20 K for the mixed layer temperatures at the two locations) is essentially the same as seen in the observations. The reason for this is simple: since the surface air temperatures are nearly identical at locations C and G, and the air temperature within a convectively mixed layer must decrease with height at the dry adiabatic lapse rate, the difference in air temperature between the two profiles must be a constant for altitudes that are within the CBL for both locations. The magnitude will be equal to the difference between the surface elevations times the dry adiabatic lapse rate. The temperature structure of the CBL is sufficiently resolved in radio occultation experiments for model comparison, and in this comparison we see that the OSU MMM simulates the observed structures quite well.

When a horizontal difference in air temperature exists, a horizontal difference in the pressure scale height exists. If this horizontal difference in air temperature exists over a
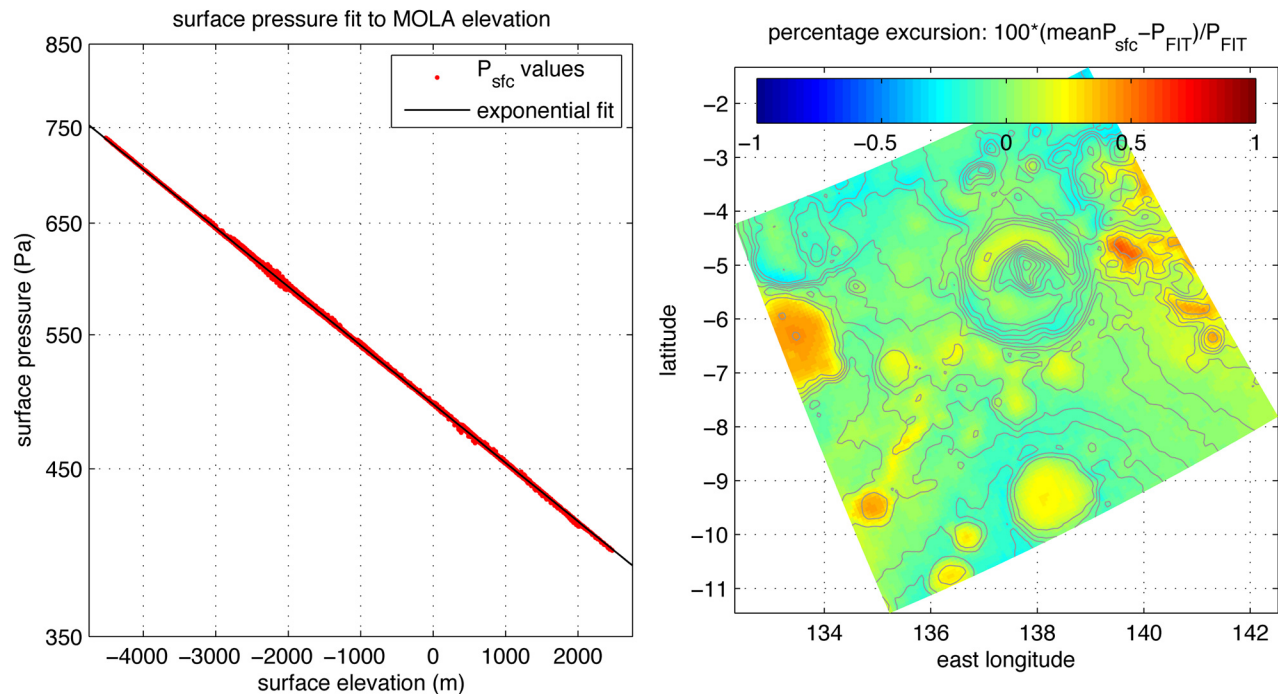
Figure 7. In the left subplot, the 20-sol diurnal mean surface pressure field from the 4 km nest (red dots) is fit to the nest topography with an exponential relationship (black line). The y-axis is a log axis. In the right subplot the percentage excursion of the mean surface pressure from the fit is shown (Figure07.jpg).

significant vertical distance, a horizontal pressure gradient must exist. And, since lower air temperatures are seen within the CBL above the lower elevation locations in Fig. 6, the pressure scale height is smaller, and the pressure will decrease more rapidly with height over these locations. In response (all else being equal), a horizontal pressure gradient develops aloft with lower pressure above the lower elevation location. Depending on the proximity of the two locations, this horizontal pressure gradient could become dynamically significant. A circulation would develop that grows stronger with the depth of the CBL, and air above the higher elevation location would accelerate horizontally towards the lower elevation location. When the 5 km profile is compared to locations near Gale Crater (seen most clearly for B and C in Fig. 6), the ellipse center profile is also seen to exhibit this characteristic difference in air temperature.

It is noteworthy that the vertical structure of the 5 km ellipse center profile (with negligible CBL depth, that is not essentially bi-modal in lapse rate like the other profiles) is similar to some in Figs. 2a and 2c of Hinson et al. (2008). A logical explanation is that these somewhat different Radio Science profiles are modified by local dynamics, circulations excited by significant changes in the local topography. An analysis of model air pressure data on constant height surfaces (not shown) does show that horizontal pressure gradients form near the surface at crater rims. However, when this analysis is performed ~2-3 km AGL, the signal becomes much weaker, and difficult to distinguish from "noise" in the model results.

It is worth mentioning that model temperature profiles

exhibit surface superadiabatic layers much deeper than those seen on Earth. Radio Science cannot resolve these layers reliably; however, the Mini-TES observations of the Mars Exploration Rovers have shown they do exist (Smith et al., 2006). Mini-TES observations were made slantwise, so it is difficult to use them to describe the superadiabatic surface layer accurately over the entire period from early morning through middle afternoon. Mesoscale model PBL schemes tend to maintain this highly unstable surface layer structure during the growth phase of the CBL, and vertical mixing within this layer would be quite vigorous. If PBL schemes are performing realistically, and convergence and divergence zones in the near surface wind field play an important role in forcing vertical motions in the atmosphere, better observations of the atmosphere very near the surface would help to constrain important dynamics. For research in the present-day, comparison between mesoscale and Large-Eddy Simulation (LES) models is one way to explore the performance and validity of PBL schemes used in mesoscale models of the Martian atmosphere (Tyler et al., 2008).

Surface Pressure in the Gale Crater Region

At the landing ellipse center in the 4 km nest, the surface pressure varies by ~11% over the diurnal cycle. This range is very similar to that of the other mesoscale models described by Haberle et al. (2012). When compared with the range of record sea level atmospheric pressure observations on Earth, the diurnal surface pressure cycle at Gale is fully half as large; and, for terrestrial storms, only the very strongest (hurricanes) can even compare to this diurnal amplitude. That the amplitude of the diurnal surface
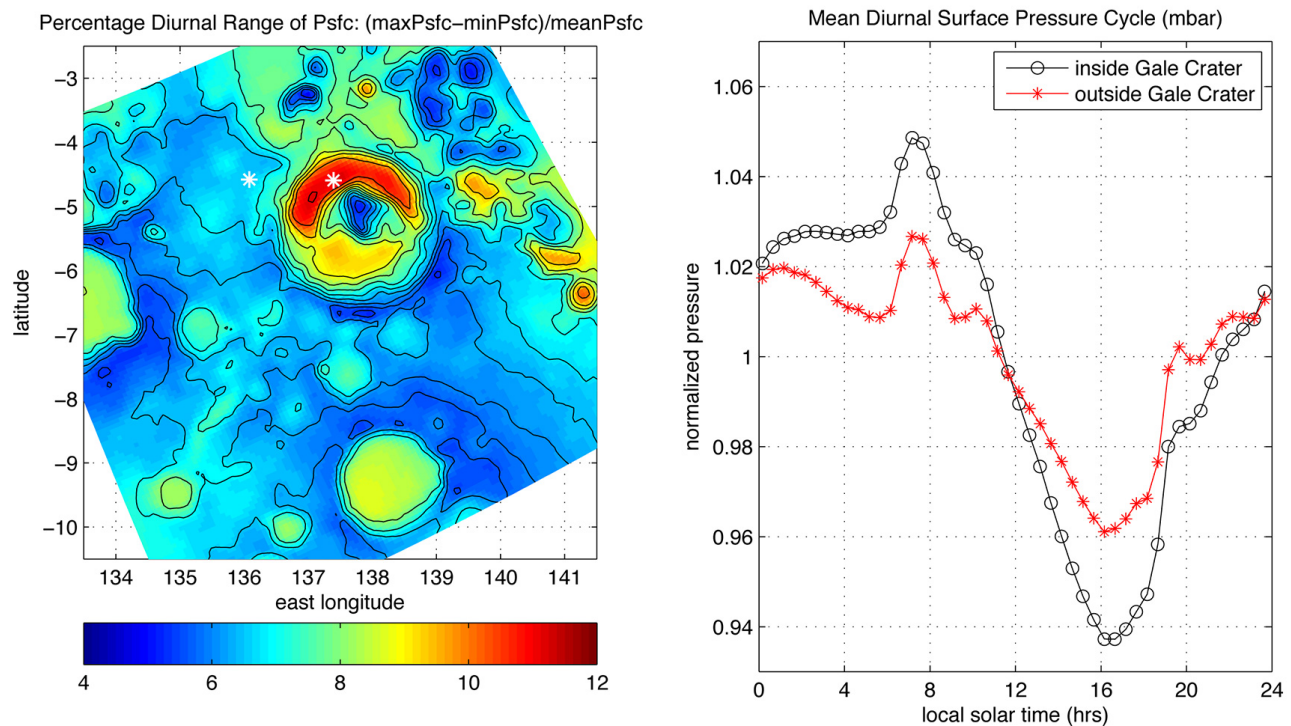
Percentage Diurnal Range of Psfc: (maxPsfc−minPsfc)/meanPsfc

Mean Diurnal Surface Pressure Cycle (mbar)

Figure 8. The 20-sol mean percentage range of the normalized diurnal surface pressure cycle is shown in the left subplot for the 4 km nest. The white asterisks in the left subplot mark the locations for the surface pressure cycles shown in the right subplot (Figure08.jpg).

pressure cycle on Mars is so large has been known for some time (Hess et al. 1977). The diurnal variation of surface pressure is primarily caused by two factors that interact and modify the vertical column of mass per unit area: 1) thermal tides in the atmosphere, and 2) the diurnal cycle of winds much nearer the surface (through convergence and divergence). In the context of spacecraft EDL, an accurate knowledge of surface pressure variation can be crucial (Vasavada et al. 2012). In this section, towards a more complete understanding of the dynamics of the Gale Crater circulation, we examine the surface pressure cycle.

When comparing GCM surface pressure predictions with mesoscale models, the interpolation of surface pressure from a GCM that does not resolve Gale Crater, to that of a mesoscale model that does resolve it (or vice versa), poses numerous challenges. Primarily, this is because the greatest air temperature changes occur nearest the ground. With the amplitude of air temperature variations most related to height above ground, and the vertical depth of these largest air temperature variations dependent on the elevation of the ground itself (evidenced by Fig. 6), an interpolation scheme would need to be fairly sophisticated to be reliable over any significant vertical distance. Even then, such a scheme would still not account for any local dynamics not resolved by the GCM. This makes it very unlikely that a comparison between GCM and mesoscale surface pressure cycles for a site like Gale Crater (one having been interpolated to the topographical height of the other) will be helpful beyond a comparison of diurnal mean values.

Over a relatively small region, surface pressure variations can be examined under the premise that an exponential relationship exists with surface elevation. Any significant excursions from this relationship can probably be explained by smaller-scale dynamics. An exponential fit of the 20-sol diurnal mean surface pressure field to its surface elevation is shown in the left subplot of Fig. 7. In the right subplot, the percentage difference of the surface pressure field from the fit is shown. For the diurnal mean, the highs and lows of individual surface pressure cycles (and their phases) mostly average out, and only small differences from the fit are seen, values between -0.25% and 0.5%. The largest positive differences are about twice as large as the largest negative differences, and these are seen only in craters or basins. The largest negative values tend to appear on steeper slopes. Gale Crater is different from other craters (highly asymmetric in the meridional direction), with only small differences from the exponential fit. Based on this analysis, the diurnal mean surface pressure in Gale Crater is close to the value that would be expected.

Complementary to Fig. 7, the left subplot of Fig. 8 is a map showing the percentage range of the normalized 20-sol mean diurnal surface pressure cycle for each location in the 4 km nest. The greatest amplitudes occur at the lowest elevations in Gale Crater. Two locations are identified with white asterisks (one inside Gale Crater and one slightly to the west). The surface pressure cycles at these locations are shown in the right subplot. Although Fig. 7 shows that the mean surface pressures in Gale Crater are as would be expected (a good agreement with the fit), the diurnal range of
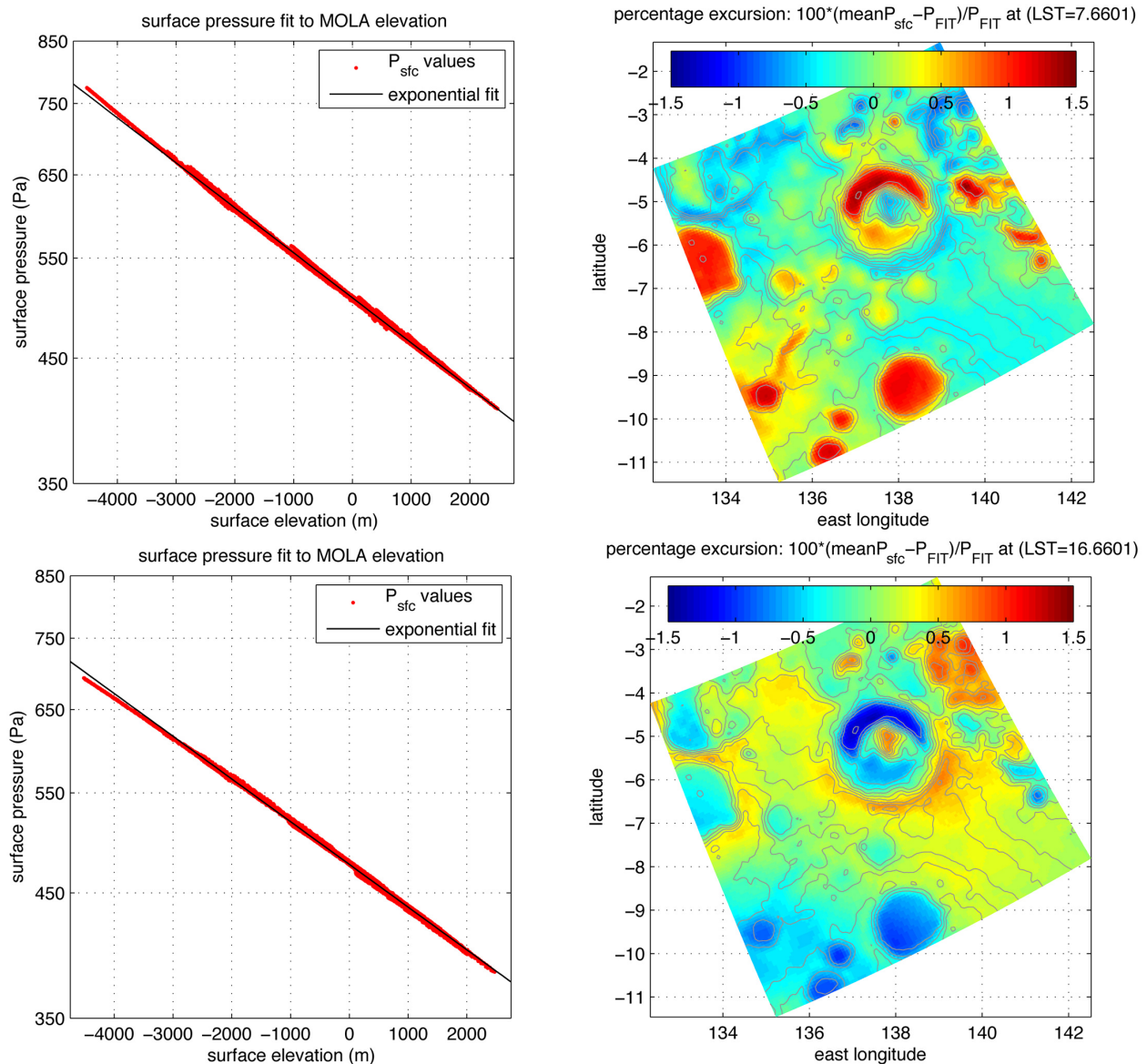
Figure 9. Percentage surface pressure excursions from the fit to topography (like Fig. 7, although an expanded color range) are shown for two times (time is true at the landing ellipse center in the 4 km nest). At these times (~0730 and ~1630), the largest differences between the surface pressure cycles in Fig. 8 are seen (Figure09.jpg). A GIF animation of the full diurnal cycle at bi-hourly intervals is available (PressureExcursion.gif).

surface pressure in the northern part of Gale Crater is generally much larger than any other location in the 4 km nest. These two locations are very close spatially, separated by only ~90 km, a subgrid distance in almost any GCM. In and/or near complex topography, attempts to reconcile the surface pressure cycles of mesoscale models with those from GCMs can be difficult and possibly quite misleading.

In a modeling context, this has an especially important dimension worth considering. Since it is difficult to eliminate reflections at the lateral boundaries of a mesoscale model mother domain (Tyler et al. 2002), there is good reason to trust the diurnal surface pressure cycle from a GCM somewhat more than that from a mesoscale model. This approach was considered primary when preparing for MSL EDL (Vasavada et al. 2012). Conversely, for a specific

location amidst highly complex topography, a mesoscale model is able to resolve local circulations with a sufficient level of realism; and, as suggested by Fig. 8, such circulations can have a surprising effect on the diurnal cycle of surface pressure. For the two specific locations in Fig. 8, the surface pressure cycles differ by ~2% in both their maximum and minimum values, with the location inside Gale Crater having a diurnal range of ~11% and the location to the west ~6.5%. A fractional surface pressure excursion of ~2%, existing over a short horizontal distance, suggests the likelihood of pressure gradients that would accelerate the flow noticeably.

The method of Fig. 7 is applied at the two times of day when the greatest differences between the surface pressure cycles shown in Fig. 8 are seen. The results are shown for both
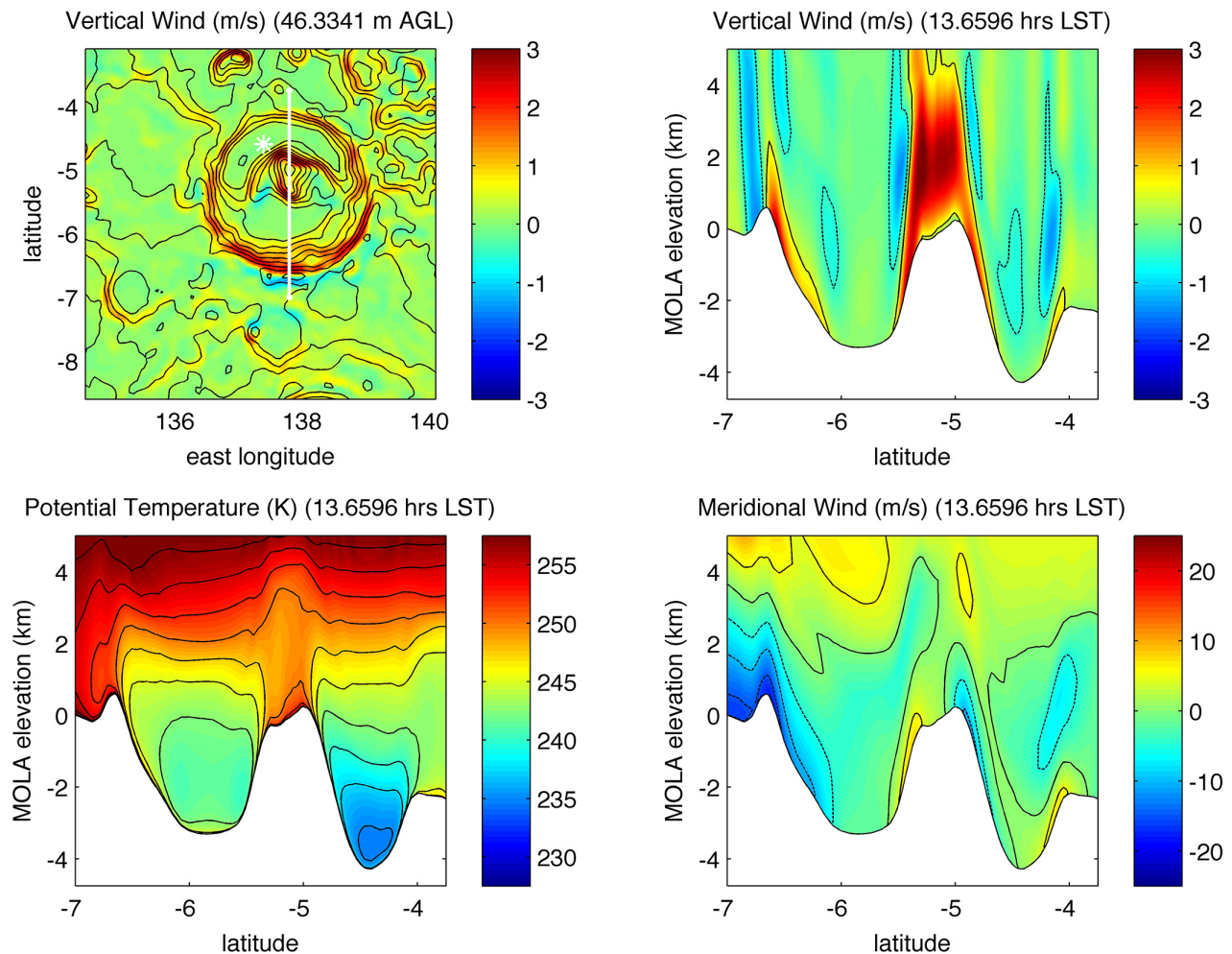
Figure 10. For a part of the 4 km nest, the upper left subplot shows constant sigma level near-surface vertical velocity (the white asterisk is at the center of the landing ellipse; the white line segment is the surface transect for the data in the other subplots). The subplots show slices of vertical velocity, potential temperature and meridional wind. The data are from the 20-sol mean diurnal cycle at ~1330 hrs LTST (true at the landing site ellipse center). Topography is shown at 500 m intervals in the upper left subplot, and 6.1 mbar is the reference pressure for the potential temperature (Figure10.jpg). A GIF animation of the full diurnal cycle at bi-hourly intervals is available (CenterCrater.gif).

times in Fig. 9. For the morning time (~0730 LTST, upper subplots), and for the largest pressures inside Gale Crater, the actual surface pressure values are greater than the fit in the upper left of the left subplot. Amplitudes of the excursions are ~10 Pa. These surface pressures cause the large positive excursions (~1.5%) seen in Gale Crater at ~0730 LTST. For the afternoon time (~1630 LTST, lower subplots), the actual pressures are smaller than the fit, and the opposite effect is seen. Comparing the two times, the excursions from the fit are close to negatives of each other, although the positive excursions in craters and basins are somewhat larger in amplitude, as the diurnal mean analysis of Fig. 7 might suggest. The best example of this is the crater on the western boundary (at ~6.5°S), where the large positive amplitude of Fig. 7 may be due to the larger morning (positive) than afternoon (negative) excursion seen in Fig. 9. Nevertheless, amplitudes of the OSU MMM excursions are in reasonable agreement with the analysis of OMEGA data described by Spiga et al. (2007).

The morning and afternoon times of Fig. 9 are important transition times in the surface wind field, which is readily seen in an animation showing the entire diurnal cycle of surface winds (SfcWinds4km.gif). At the morning transition time the ground has begun to warm and crater slope flows are switching to upslope, whereas for the afternoon time the ground has begun to cool and crater slope flows are switching to downslope. The phase of the dichotomy boundary slope flows is not identical to that of the crater slope flows. Moreover, the dichotomy boundary slope flows do not reach maximum upslope or downslope strength at the same time of day at all locations along the topographical gradient of the dichotomy boundary, adding complexity to an already complex circulation. At this point, to better understand the dynamics involved, and to understand how CBL depths and local surface pressure cycles are modified, the vertical dimension of the circulation is considered.
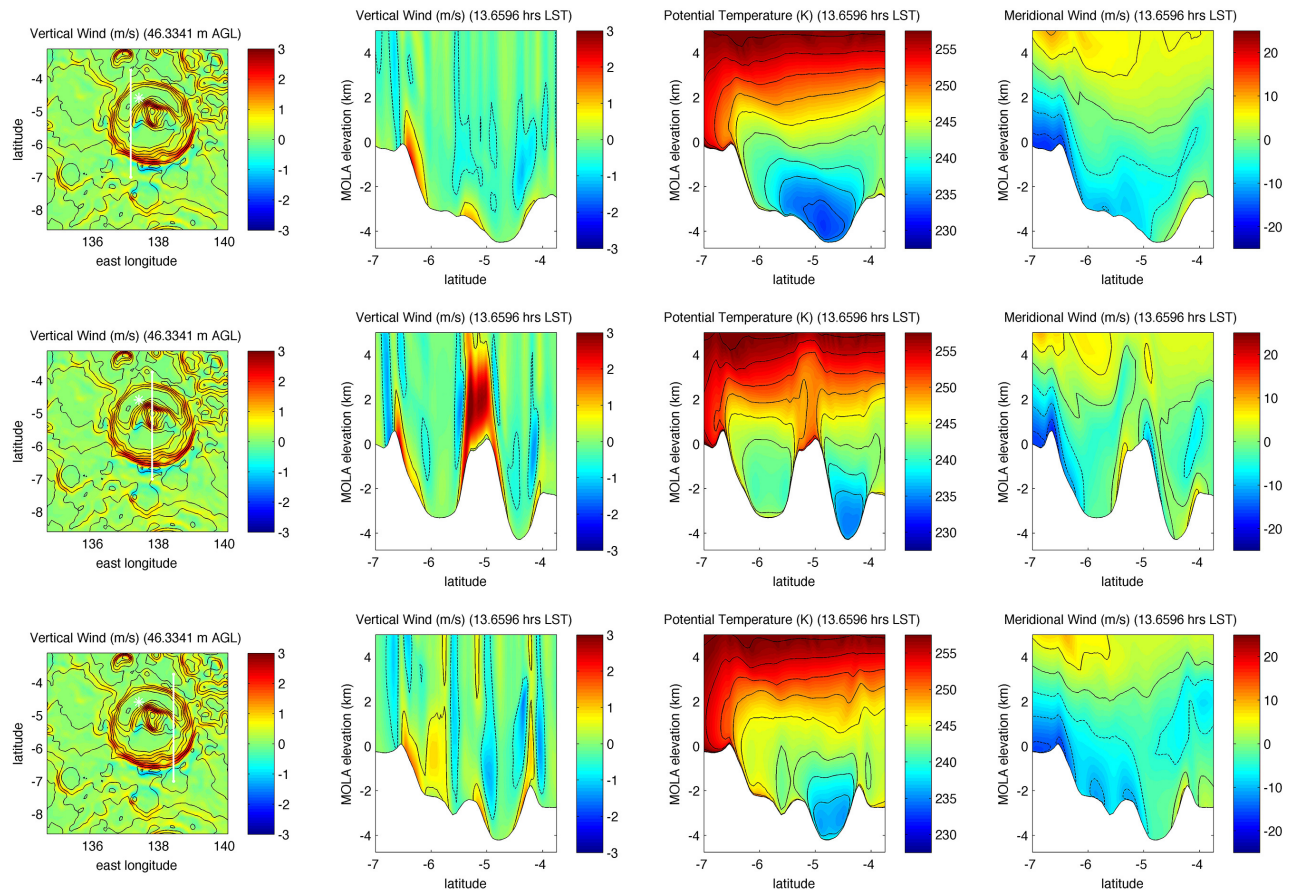
Figure 11. The data of Fig. 10 (middle subplots) is compared with data at two additional locations. The two new transects are located 0.65° to the east and west of the Fig. 10 transect (Figure11.jpg). GIF animations of the full diurnal cycle at bi-hourly intervals are available (WestCrater.gif, CenterCrater.gif and EastCrater.gif).

The Gale Crater Circulation

Examination of Figs. 5, 8 and 9 shows that the northern half of Gale Crater has: 1) very small CBL depths, 2) a much larger amplitude for the surface pressure cycle than is seen outside the crater (or even in the southern half of the crater), and 3) much larger excursions from the expected surface pressure cycle than are seen in the southern half of the crater or elsewhere in the domain.   There is a good spatial correlation between these various aspects of the diurnal circulation, although the very small CBL depths correlate somewhat better with albedo, while the features in the surface pressure field correlate best with the lowest elevations in the northern part of the crater. Slope flow on the southern crater rim wall is typically in the same direction as that forced by the dichotomy boundary, while at the north rim, due to the anti-parallel nature of the slopes, the forcings are always in opposite directions.   If the timing of the maximum strength in the upslope and downslope flow of these two forcings were identical at both rims, interactions between them would always be constructive at the south rim and destructive at the north. As seen in Fig. 4, the timing is

not identical. In the three subsections that follow, to develop a more complete understanding of the dynamics of this complex circulation, we examine the vertical dimension of the circulation.

Daytime Atmospheric Slices Across Gale Crater

We begin with early afternoon slices of the 20-sol mean diurnal cycle meteorology above a south to north transect that passes directly over Mt. Sharp. The upper left subplot of Fig. 10 shows constant sigma level near-surface vertical velocity (useful for locating strong slope flows), as well as the surface transect location. The three other subplots show vertical velocity, potential temperature (for a 6.1 mbar reference pressure), and meridional wind velocity for a time of ~1330 LTST at the landing ellipse center. At the walls of Gale Crater and on the slopes of Mt. Sharp, the flow is upslope, as can be seen in the meridional wind field and both vertical velocity subplots. The vertical velocity slice shows a strong updraft feature directly over Mt. Sharp. This updraft modifies the potential temperature field, causing constant temperatures over a vertical depth of ~3 km, the signature of a well-mixed region where the CBL is growing towards the

maximum of ~4 km seen in Fig. 5. In the northern half of the crater, no well-mixed layer develops, and potential temperatures are noticeably cooler than in the southern part. The cooler daytime temperatures are related to the much brighter albedo of the northern crater floor (see Fig. 3). In the meridional wind field of Fig. 10, the flow is everywhere upslope on the rim walls of Gale Crater and the slopes of Mt. Sharp. The flow up the south rim wall is much stronger and deeper than the flow up the north rim wall. On the slopes of Mt. Sharp the meridional wind is also stronger on the northern side. Gale Crater is certainly not symmetric, so we would not expect the meridional circulation to be. At this time, the regional flow up the dichotomy boundary is growing strong, and the meridional wind shows this. To the south of the south crater rim, the dichotomy upslope flow is strong. Flow up the south rim wall appears to be "feeding" the dichotomy boundary upslope flow.

Since upslope flows move mass up both crater walls as well as up both sides of Mt. Sharp, conservation of mass requires a return flow. The vertical velocity subplot suggests that (at least in part) this return flow is provided by subsidence over the floor of the crater; this is most significant over the northern crater floor. It is noteworthy that the most favored locations for subsidence are south of the upslope flows (or updrafts), south of the plume over Mt. Sharp and south of the flows up both crater rim walls. Over the north rim a minimum is seen in the meridional wind. This feature is part of the dichotomy boundary upslope flow, and is co-located with a strong subsidence feature in the vertical velocity. When the potential temperature slice is considered along with the winds, we see that the meridional wind brings air in over the northern crater floor, where it encounters the downdraft and warms adiabatically in subsidence. This displaces the warmer potential temperature surfaces towards the ground and increases the stability of the air column. Over the northern crater floor, this effect is greatest near the north crater rim; over the north side of Mt. Sharp, potential temperature surfaces are displaced upwards by the strong upslope flow. These aspects of the circulation significantly modify the temperature structure. With subsidence velocities in excess of ~0.6 m/s over a sizeable part of the northern crater floor, adiabatic warming rates of ~9 K/hr (adiabatic lapse rate of 4.3 K/km following the air parcel) will be seen. It is important to note that the meridional flow does not cross Mt. Sharp.

A more complete depiction of the flow at this time of day requires an examination of the meteorology that is slightly to the east and west of the central slice (as used in Fig. 10). Two additional transects are examined; each is located 0.65° of longitude (~38 km) from the central transect. The meteorology over all three transects is shown in Fig. 11. In all cases, the vertical velocity field shows subsidence over the northern floor of Gale Crater. This subsidence is a widespread phenomenon, and the increased stability it causes in the air column is almost certainly playing an important role in inhibiting the growth of the CBL. When animations that show the entire diurnal cycle of the data for each slice in Fig. 11 are examined (WestCrater.gif, CenterCrater.gif and

EastCrater.gif), it is clear that this subsidence is not limited to a short time window. This subsidence is providing a basic mass-conserving return circulation to the upslope flows along the crater rim walls and on the slopes of Mt. Sharp. A significant CBL cannot form over the northern crater floor because of two factors: 1) the air temperatures aloft are warming fast enough to keep the air column stable; and, 2) the elevated albedo values of the northern crater are sufficiently effective in limiting the energy absorbed by the ground. The very good correlation between the higher albedo values and the smallest CBL depths underlines the importance of the albedo.

The local circulation near the north crater rim exhibits the primary elements of a circulation that was proposed in the discussion of Fig. 6 above. There is a sharp difference in CBL depths (seen in Fig. 5 as well as in the potential temperature slices of Fig. 11). And, because horizontal differences in temperature exist over a significant vertical depth, a horizontal pressure gradient must also exist. The pressure gradient would be in a direction that would support (accelerate) the minimum seen in the meridional wind field over the crater rim. Importantly, the return flow circulation that forms is favored by the weak dichotomy boundary upslope flow (in opposition to the flow up the north rim). In that the meridional flow does not continue across Mt. Sharp in the central slice, subsidence is again favored.

For the slices to either side of Mt. Sharp, the stronger upslope dichotomy boundary flow is seen much further north into Gale Crater. Although the meridional flow in these two slices is weaker to the north, it does exist across all latitudes of Gale Crater, unlike the meridional flow of the central slice. Mt. Sharp (as well as the afternoon convective plume above it) provides an obstacle to the development of uniform upslope flow across Gale Crater; the northern part of Gale Crater can be seen as being effectively "shielded" from this strong regional flow. Because of the zonal variation in the meridional wind, consideration of the zonal wind is important before drawing definitive conclusions. However, an examination of zonal winds (not shown) reveals that zonal wind speeds are small almost everywhere, less than ~5 m/s with very little variation across the three slices that would suggest zonal wind is playing an important role. This is especially so in the northern part of Gale Crater. The dynamically important part of the horizontal wind field is the meridional wind. This result is logically consistent with the asymmetries of Gale Crater (topography and albedo), which exist primarily in the meridional direction, aligned with the topographical gradient and the slope flow forcing along the dichotomy boundary.

One feature worth discussing is seen in the southern part of Gale Crater. In Fig. 11, the vertical velocity is significant over a depth of ~4 km southeast of Mt. Sharp. This is where the largest CBL depths in Gale Crater are located (Fig. 5). This updraft feature is excited by convergence in the wind field near the surface. This convergence can be seen to evolve during the afternoon hours in the SfcWinds4km.gif animation. It occurs where the flows up the topographical
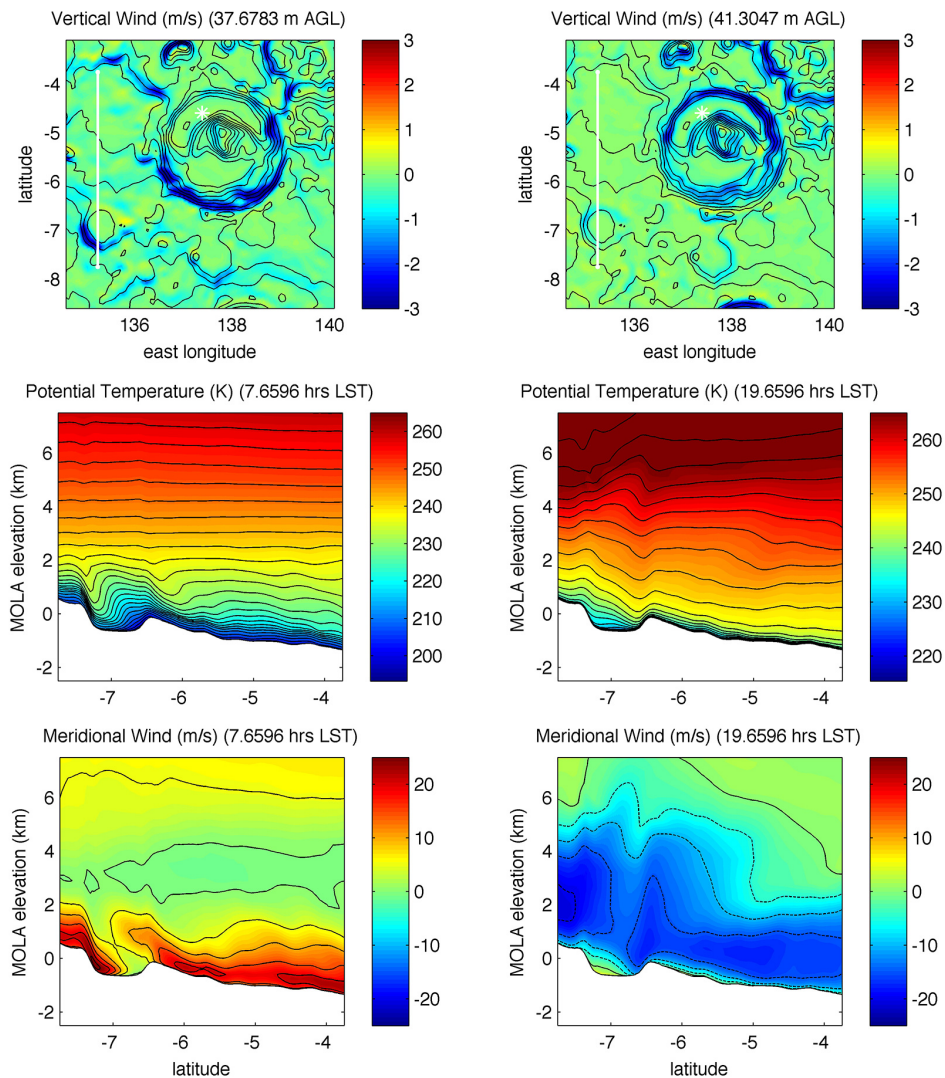
Figure 12. For the dichotomy boundary slope flows, the upslope and downslope maxima are shown at a location to the west of Gale Crater. The upper two subplots show the transect location and the constant sigma near-surface vertical velocity at the two times indicated in the lower subplots (time is true at the landing ellipse center, shown with a white asterisk). The lower subplots are potential temperature and meridional wind (Figure12.jpg). A GIF animation of the full diurnal cycle at bi-hourly intervals is available (FarWest.gif).

shelves (from the lower north to the higher south) meet behind Mt. Sharp. The flow up the western shelf wraps around Mt. Sharp to provide the strongest zonal winds in the crater, becoming weak where the two flows meet at the top of the eastern shelf. Given the location of this convergence feature and the correlation with CBL depths, differences in insolation at the surface (due to the albedo gradient in the southern crater floor) are playing a role.

The Dichotomy Boundary Slope Flows
To better understand the diurnal cycle of the dichotomy boundary slope flows, and the phase relationship to the slope flows in Gale Crater, we examine two times of day at a transect located west of Gale Crater in Fig. 12. At these two times, the slope flows up and down the dichotomy boundary are the strongest. The downslope maximum occurs at ~0730

LTST and the upslope maximum occurs at ~1930 LTST. At other locations along the dichotomy boundary near Gale Crater the timing of the maxima is similar. On this specific transect the topographical gradient is fairly constant, although a crater at the south end provides some variation. At both times of day, we find that the flow is highly modified by the topography of this rather generic crater.

As with Figs. 10 and 11, the upper subplots of Fig. 12 show the constant sigma level near-surface vertical velocity from the 20-sol mean diurnal cycle. For the two times of day shown, ~0730 LTST is the time of the surface pressure excursion maximum in Fig. 9. At this early morning time, strong slope flow is seen on the south rim of Gale Crater in Fig. 12, while there is almost no flow on the north rim. By early evening, at ~1930 LTST, three hours after the surface pressure excursion minimum in Fig. 9, the situation is basically reversed. At both of these times, the slope flows at
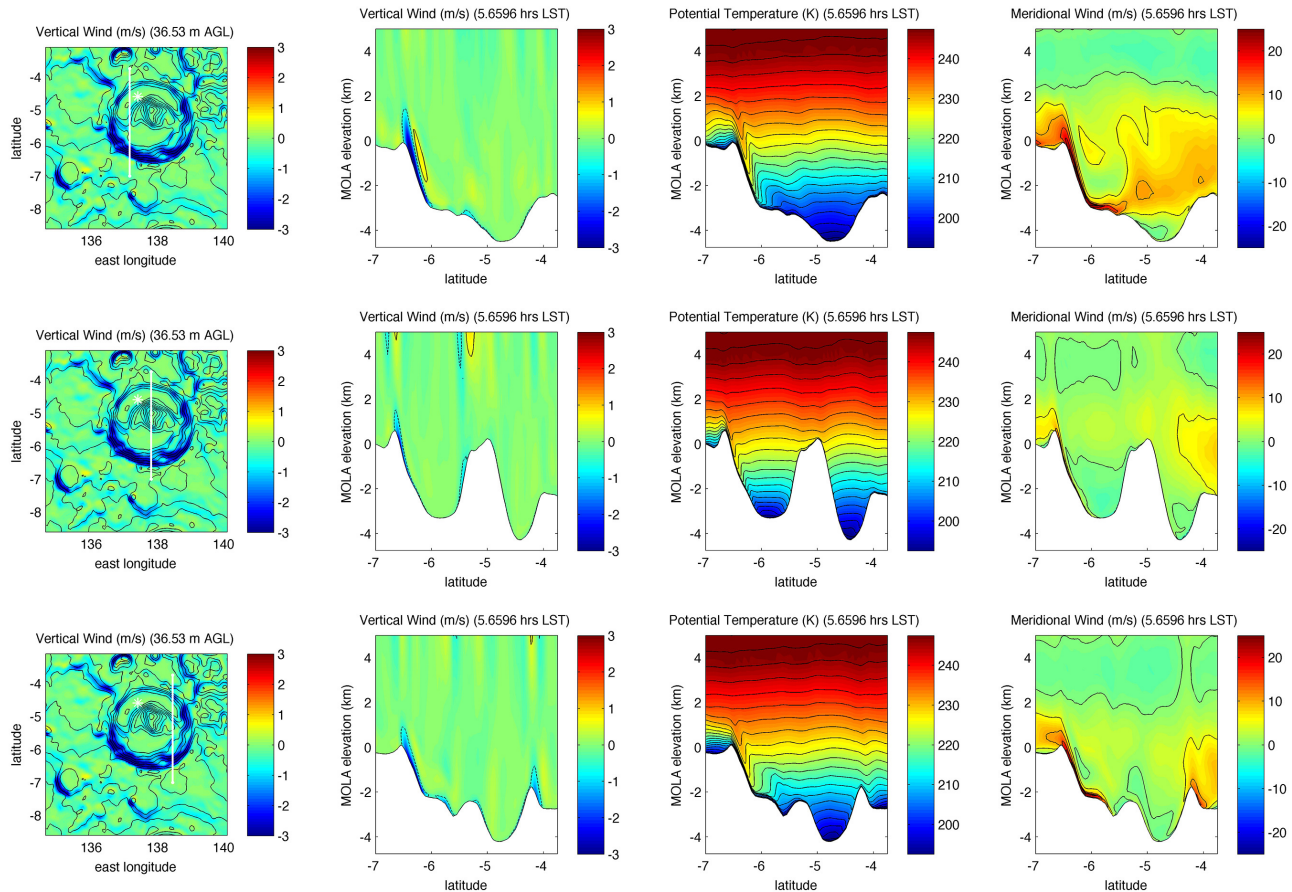
Figure 13. At the early morning time of ~0530 LTST (true at the landing ellipse center), atmospheric slices of model data are compared at the same locations that were used in Fig. 11 (Figure13.jpg). GIF animations of the full diurnal cycle at bi-hourly intervals are available (WestCrater.gif, CenterCrater.gif and EastCrater.gif).

the north and south rims of Gale Crater differ greatly because the dichotomy boundary and crater slope flows interact and have different phases. The crater slope flow forcing is weak and in transition at both times of day, switching direction in response to the ground temperature just warming above the air temperature or having just cooled below it. That these two times are essentially transition times is further evidenced by the minimal flow on Mt. Sharp. Therefore, the dichotomy boundary flow is generally strongest when slope flow on the crater rim walls is weakest, and would easily overwhelm any weak flow (constructively or destructively) at these times. These transition times are dynamically significant; their exact timing is immediately after the two surface pressure excursion maxima shown in Fig. 9, good evidence for a dynamical relationship.

Upon examining the lower subplots in Fig. 12, three points are worth making. The first is that the mean depth of upslope flow is generally ~2-3 times as deep as the nocturnal drainage flow (buoyancy enhances vertical mixing during daytime convection). The second is that at both times of day the strong flow can be seen to excite stationary gravity waves

due to the topography of the crater. For the downslope case, the stationary gravity wave is seen to develop north of the north crater rim, where the upwind tilt in the potential temperature field marks its location and vertical extent. For the upslope case, the stationary gravity wave has a vertical extent of ~5 km, and forms directly over the north crater rim (again identified by the upwind tilt in the potential temperature field). Since the depth of the upslope dichotomy boundary flow is about twice as deep over the crater, the gravity wave in the upslope flow is effectively mixing momentum in the vertical. The third point is seen in the nocturnal drainage flow entering the crater from the south. In response to the additional slope flow forcing of the crater wall, the drainage flow accelerates and wind speeds reach ~25 m/s. Then, the flow abruptly stops at the bottom of the crater, where we see potential temperature isotherms become nearly vertical. Only vigorous and turbulent mechanical mixing in the vertical can cause this sort of structure to form at night, which makes this feature look very much like a hydraulic jump. Since similarly sized craters are abundant on the dichotomy boundary, this phenomenon could be quite commonplace.

Nighttime Slices Across Gale Crater

As seen in Fig. 12, the circulation at night can be very interesting, especially in and near craters. In Fig. 13, we examine the circulation very late at night at the same three transects of Fig. 11. At this time, actually just before sunrise (~0530 LTST), the dichotomy boundary flow is strongly downslope, although it will not reach maximum strength until ~0730 LTST. Similar to how the nocturnal drainage accelerated into the crater of Fig. 12, the flow down the south wall of Gale Crater becomes much stronger in both the meridional and vertical wind along all three transects. For the western transect, the 20-sol mean diurnal cycle meridional wind speeds reach ~35 m/s. Even when considering the hydrostatic dynamics being used in the OSU MMM, as well as the need for increased horizontal resolution to resolve such structures, the simulated flow is highly consistent with a hydraulic jump. This conclusion is supported by the fact that the vertical gradient of potential temperature becomes negative towards the end of the jet in the near-surface winds. Zonal winds are very weak (again not shown), having little importance dynamically. The western side of Gale Crater is favored for this strongest flow, a consequence of the local topography and the location of Gale Crater on the dichotomy boundary. The topographical height of the southern crater floor is similar to the top of the northern rim. With a very stable atmosphere over the northern crater floor, helped by the adiabatic warming that the air undergoes in flowing down the south rim, the flow separates from the surface after the hydraulic jump, becomes much deeper through turbulent mixing in the vertical, and continues northward as part of the dichotomy boundary nocturnal drainage. As with the daytime case of Fig. 11, the central slice in Fig. 13 is where the dichotomy boundary flow is weakest, especially so over the northern part of Gale Crater.

For the present day climate of Mars, hydraulic jumps are likely to be an every day phenomenon. Near the equator where the duration of night and day is always similar, strong upslope and downslope flows will always form. Aeolian erosion could be enhanced by orders of magnitude locally, having a dramatic effect over longer timescales. As suggested by Kite et al. (2012), Mt. Sharp and the present day topography of Gale Crater may be a consequence of aeolian processes related to slope flows. The albedo feature in and to the south of Gale Crater (see Fig. 3), which reaches much higher up the dichotomy boundary, is itself highly suggestive of aeolian processes.

Surface Pressure and Air Temperature

In the hydrostatic atmosphere of the OSU MMM, surface pressure excursions form in response to modification of the vertical profile of air temperature. To describe actual surface pressure excursions (such as modeled in the northern part of Gale Crater), the hydrostatic assumption is quite sufficient. Then, for a surface pressure excursion to form, the temperature profile of the air column would differ from an unmodified "typical" temperature profile at that time of day, where the vertical profile of air temperature is most strongly (or typically) related to elevation above the local topography. An understanding of this "typical" relationship, between temperature and height above the ground, is very useful for improving the initial condition of a mesoscale model simulation when the data must be interpolated from coarse GCM output (Tyler et al. 2002). Under the presumption that there is a viable relationship between topography and surface pressure, Fig. 9 tells us that some locations (at some times of day) have vertical profiles of air temperature that must differ significantly from a "typical" temperature profile. With this, the vertical profile of the pressure scale height varies from "typical" and a surface pressure excursion develops. The exponential fit of surface pressure to topography, which was used to construct Figs. 7, 8 and 9, essentially relies upon such excursions being rare (the "fit" subplots of Figs. 7 and 9 show this). In focusing on the largest excursions in the northern floor of Gale Crater, we can describe how the vertical temperature structure is modified from "typical".

During the day, widespread subsidence occurs over the northern floor of Gale Crater. The increased atmospheric stability caused by this subsidence plays an important role in inhibiting the development of a normal CBL. During the night, nocturnal drainage brings air down into the northern crater floor. For mass conservation, upwelling must occur, and this can be detected in each of the three vertical velocity slices shown in Fig. 13. In both cases (day and night), vertical motion modifies the vertical temperature structure adiabatically in an environment that is "shielded" from the scouring effects of the dichotomy boundary slope flow. Over the northern part of Gale Crater during daytime, subsidence displaces the potential temperature surfaces towards the ground (Fig. 11). At night, upwelling displaces the potential temperature surfaces upwards (Fig. 13). With this, the actual air temperature profiles become correlated less with elevation above the local topography and more with elevation above a mean regional topography. In both cases, for the actual air temperatures, the vertical distance between near-surface isotherms increases, forming a relatively deep warmer/cooler layer during day/night. As a result, the vertical temperature structure adopts the vertical relationship to the regional topography more rapidly, where the tendency for isotherms to follow the local topography disappears more rapidly in the vertical than if the air column were unaffected by the local dynamics. This can be seen in Fig. 14, where the actual air temperature is shown at the two times of day when the surface pressure excursions are largest over the northern floor of Gale Crater. At both times, the isotherms over the northern part of Gale Crater in Fig. 14 are highly similar in elevation to those north of the crater, whereas for the southern part of Gale Crater, this is not the case. We also note the greater distance between isotherms within the northern part of the crater (compared to the southern part) that allows the relative warming above a "typical" profile or cooling below it to happen. The surface pressure excursion at these times reflects the modified profile of pressure scale height. Over the lowest elevations in the northern part of Gale Crater, dynamics of the local circulation cause significant modification of the vertical temperature structure. The effect on the CBL depth and the diurnal surface pressure
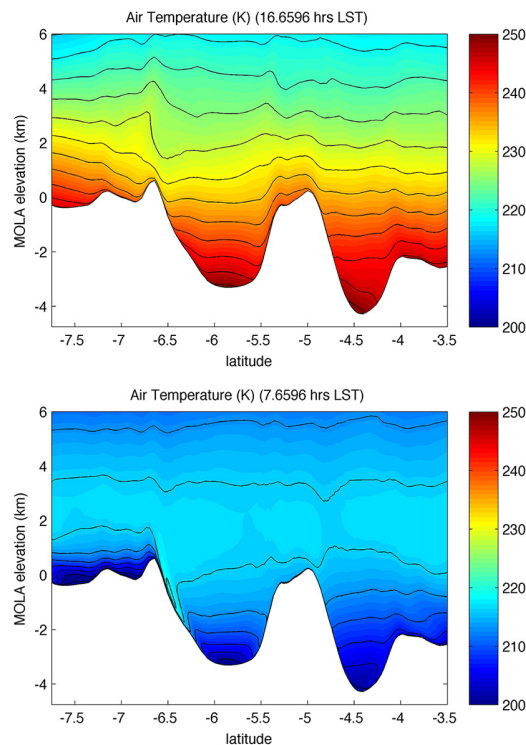
Figure 14. For the central slice of Figs. 11 and 13, the air temperature is shown for the two times o day when the surface pressure excursions are largest, ~0730 LTST and ~1630 LTST (valid at the landing site ellipse center) (Figure14.jpg).

cycle is seen to be significant.

Summary and Conclusion

The OSU MMM is one of two mesoscale models involved in extensive atmospheric modeling that was performed in support of MSL EDL (Vasavada et al. 2012). A concerted effort was undertaken to tune model results to observational data, and results from the two primary models were regularly compared. Using multiple levels of nesting, numerous candidate sites were examined at high resolution. In general the models were almost always in good qualitative and even quantitative agreement. For Gale Crater (the MSL landing site), Haberle et al. (2012) describe a comparison of model results that included four additional models, two GCMs and two mesoscale models. All the mesoscale models predict a similarly complex surface wind circulation in Gale Crater. In this work, results from the OSU MMM are used to explore the dynamics of the diurnal circulation in and near Gale Crater. We investigate: 1) the very small CBL depths modeled over the northern crater floor, 2) the large surface pressure excursions seen there, and 3) the role of the slope flows excited by the dichotomy boundary and the slopes of the crater rim walls and Mt. Sharp.

The location of Gale Crater on the dichotomy boundary is very important for the resulting circulation. Flow up and down the dichotomy boundary is an integral part of the diurnal cycle of wind in the region and in the crater. Within Gale Crater, the crater rim walls and Mt. Sharp excite vigorous slope flows. Because of the steeper slopes inside

Gale Crater, these flows initiate more rapidly and become quite strong. At the south rim, the rim wall and the dichotomy boundary slope flow forcings would presumably add in a constructive way, whereas for the north rim their interaction would in general be destructive (a conclusion based simply on parallel or anti-parallel slopes). The actual timing of the two slope flow forcings is such that the dichotomy boundary flows are at their maximum strength when the crater slope flows are at their weakest and in the process of reversing direction (see Fig. 12). The intra-scale interaction between these two slope flow forcings causes the transitions between upslope and downslope flow to occur at different times at the south and north rims. Deep within Gale Crater the near surface circulation is primarily driven by the local slope flow forcings (this is especially so in the low northern part). In the southern part of the crater, and/or above the surface or nearer the crater rims, the larger-scale slope flow along the dichotomy boundary is seen to play an important role. Gale Crater itself is complex, with significant meridional asymmetries in its topography and albedo (see Fig. 3). When the circulation of the entire crater is considered, these asymmetries play an important role. Mt. Sharp is dynamically important in multiple ways.

Mt. Sharp excites slope flows that are an integral part of the crater circulation. During the day, upslope flows on Mt. Sharp and the crater walls necessitate a return flow for mass conservation. Over the northern crater floor this is provided by widespread subsidence (see Figs. 10 and 11). That the northern crater floor is most affected by subsidence is a consequence of how the developing dichotomy boundary

upslope flow interacts with the upslope flow at the north rim of Gale Crater. At the north rim, this interaction is part of a smaller-scale circulation that enhances subsidence over the northern crater floor. Subsidence displaces the potential temperature surfaces downward, enhancing atmospheric stability to become a primary dynamical factor in inhibiting CBL growth over the northern crater floor. Since a very good correlation also exists between albedo and the smallest mixed layer depths over the northern crater floor, the much brighter albedo values are certainly playing an important role in reducing heating of the ground. Due to subsidence warming of the air column, paired with diminished heating of the surface (larger albedo values), growth of the CBL is essentially prohibited over the northern crater floor. Albedo has an important effect on local dynamics elsewhere. Convergence features, correlated with albedo gradients in the south part of Gale Crater and to the south of Gale Crater, are seen to cause strong updrafts that have an important effect on the local CBL (SfcWinds4km.gif and Fig. 5).

During daytime a plume of rising air develops over Mt. Sharp. We find that both Mt. Sharp and this plume interfere with the ability of the dichotomy boundary slope flow to develop over the entirety of Gale Crater. This regionally forced slope flow is generally weaker over Gale Crater, and essentially nonexistent over the central northern part. The northern part of Gale Crater is "shielded" from the scouring effect of this regional slope flow. With this "shielding", mass-conserving return circulations (of moderate strength as just described) can become meteorologically important. It allows the vertical structure of air temperature over the northern crater floor to become significantly modified, as shown in Fig. 14. The modified temperature structure changes the pressure scale height profile, which leads to the large negative daytime surface pressure excursion seen in Fig. 9.

After sunset, nocturnal drainage down the north crater rim wall and down the slopes of Mt. Sharp contribute in the accumulation of cold air over the northern crater floor. In a mass-conserving return circulation, the air over the crater floor rises and cools adiabatically. The air mass above the northern crater floor is also "shielded" by Mt. Sharp from the strong nocturnal drainage along the dichotomy boundary at night; this allows the adiabatic cooling to become important for the local meteorology (Figs. 13 and 14). In response, the local pressure scale height becomes smaller, which causes the large positive nighttime surface pressure excursion that reaches its maximum at ~0730 LTST (Fig. 8).

At both times of day, when the surface pressure is most affected, the vertical temperature structure is better described by elevation above the mean regional topography, a relationship with the vertical that is more terrestrial than Martian in nature. Local dynamics cause this to happen most dramatically in the northern half of Gale Crater; elsewhere (where dynamical modification is weaker or washed away by strong winds) the isotherms tend to maintain a more "typical" Martian relationship to height above local topography. Further analysis of this kind of circulation (at

other sites) could possibly be used in a novel approach to explore radiative and dynamical timescales for the mesoscale on Mars. In general, since horizontal pressure gradients must form as CBL depths vary with the height of the topography, and strong slope flows on Mars must be ubiquitous, all craters and basins will be subject to these effects. However, due to the uniqueness of Gale Crater, its location on the dichotomy boundary, and the importance of Mt. Sharp in "shielding" the northern part of the crater, the combination of forcings is able to produce a complex structure of surprising anomalies in CBL depth and surface pressure in primarily the northern crater basin. Since the largest surface pressure excursions in the northern crater basin begin declining at the same time of day that the crater slope flows are in transition, the dynamical link appears to be clear.

Other craters and basins are seen to have smaller CBL depths and larger diurnal cycles of surface pressure than their surroundings. The aspect ratios and the horizontal scales of craters must be important, since very little effect would seem possible for a very large crater with a shallow rim; in this case the vertical temperature structure would maintain the "typical" vertical structure (strongly related to height above the local topography), as dominated by radiative forcing. Modeling efforts have previously shown that these effects can be dramatic for large basins such as Valles Marineris (Tyler et al. 2002 and Rafkin and Michaels, 2003). In this work and other modeling for MSL EDL, such effects appear regularly at the much smaller scales examined here; this is nicely supported by the OMEGA observations described by Spiga et al. (2007). An exploration of the important spatial and temporal scales is left for future study.

Finally, the superposition of downslope dichotomy boundary flow with the flow down crater rim walls can produce very strong nocturnal drainage. Hydraulic jumps appear to form quite easily in this environment, and for the early morning case shown inside Gale Crater (Fig. 13), the 20-sol mean diurnal cycle winds reach ~35 m/s just upwind of the jump. If nonhydrostatic dynamics and increased resolution were used, the modeled flow is likely to be even stronger. For the equatorial location of Gale Crater, this phenomenon would not be limited to a specific season in the present day climate, and fairly significant changes in the background dust loading are not expected to have a dramatic effect on a circulation that is so strongly forced by regional and local topography. Aeolian erosion may play a very important role in shaping the surface of Gale Crater (and other craters in the region) over longer timescales.

Directory of Supporting Data

root directory
manuscript.rtf this file
Fig. 1 Figure01.jpg full-resolution image
Fig. 2 Figure02.jpg full-resolution image
Fig. 3 Figure03.jpg full-resolution image
Fig. 4 Figure04.jpg full-resolution image
Fig. 5 Figure05.jpg full-resolution image
Fig. 6 Figure06.jpg full-resolution image

Fig. 7 Figure07.jpg full-resolution image
Fig. 8 Figure08.jpg full-resolution image
Fig. 9 Figure09.jpg full-resolution image
Fig. 10 Figure10.jpg full-resolution image
Fig. 11 Figure11.jpg full-resolution image
Fig. 12 Figure12.jpg full-resolution image
Fig. 13 Figure13.jpg full-resolution image
Fig. 14 Figure14.jpg full-resolution image
  ANIMATIONS
  SfcWinds4km.gif GIF animation
  PressureExcursion.gif GIF animation
  FarWest.gif GIF animation
  WestCrater.gif GIF animation
  CenterCrater.gif GIF animation
  EastCrater.gif GIF animation

References

Cantor, B.A., 2006. Mars Orbiter Camera observations of Martian dust devils and their tracks (September 1997 to January 2006) and evaluation of theoretical vortex models. JGR, (111)E12002, doi: 10.1029/2006JE002700.

Haberle, R.M., 2012. Meteorological predictions for the REMS experiment on MSL. Mars Journal, submitted.

Hess, S.L., Henry, R.M., Leovy, C.B., Ryan, J.A., Tillman, J.E., 1977. Meteorological results from the surface of Mars: Viking 1 and 2. JGR, 82:4559-4574, doi: 10.1029/JS082i028p04559.

Hinson, D.P., Pätzold, M., Tellman, S., Häusler, B., Tyler, G.L., 2008. The depth of the convective boundary layer on Mars. Icarus, 198, 57-66, doi: 10.1016/j.icarus.2008.07.003.

Hong, Song-You, Hua-Lu Pan, 1996. Nonlocal Boundary Layer Vertical Diffusion in a Medium-Range Forecast Model. Mon. Wea. Rev., 124, 2322–2339.

Kite, E.S., Lewis, K.W., Lamb, M.P., 2012. Growth and form of the mound in Gale Crater, Mars: slope-wind enhanced erosion and transport. astro-ph.EP, arXiv:1205.6840, http://arxiv.org/abs/1205.6840.

Putzig, N.E., Mellon, M.T., 2007. Apparent thermal inertia and the surface heterogeneity of Mars, Icarus, 191, 68-94, doi: 10.1016/j.icarus.2007.05.013.

Rafkin, S.C.R., Michaels, T.I., 2003. Meteorological predictions for 2003 Mars Exploration Rover high priority landing sites. JGR, 108, E12, doi: 10.1029/2002JE002027.

Smith, M.D., M.J. Wolff, N. Spanovich, A. Ghosh, D. Banfield, P.R. Christensen, G.A. Landis, S.W. Squyres, 2006. One Martian year of atmospheric observations using MER Mini-TES, JGR, 111(E12S13), doi: 10.1029/2006JE002770.

Smith, M.D., 2006. TES Atmospheric Temperature, Aerosol, Optical Depth, and Water Vapor Observations 1999-2004. Second workshop on Mars atmospheric modeling and observations. Granada, Spain.

Spiga, A., F. Forget, B. Dolla, S. Vinatier, R. Melchiorri, P. Drossart, A. Gendrin, J.-P. Bibring, Y. Langevin, B. Gondet, (2007). Remote sensing of surface pressure on Mars with the Mars Express/OMEGA spectrometer: 2. Meteorological maps, JGR, 121(E8), doi: 10.1029/2006JE002870.

Troen, I., L. Mahrt, 1986. A simple model of the atmosphereic boundary layer: Sensitivity to surface evaporation. Bound. Layer Meteor., 37, 129-148.

Tyler, D. Jr., J.R. Barnes, R.M. Haberle, 2002. Simulation of surface meteorology at the Pathfinder and VL1 sites using a Mars mesoscale model. JGR, 107(5018), doi: 10.1029/2001JE001618.

Tyler, D. Jr., J.R. Barnes, E.D. Skyllingstad, 2008. Mesoscale and large-eddy simulation model studies of the Martian atmosphere in support of Phoenix. JGR, 113(E3), doi: 10.1029/2007JE003012.

Vasavada, A.R., Chen, A., Barnes, J.R., Burkhart, P.D., Cantor, B.A., Dwyer-Cianciolo, A.M., Fergason, R.L., Hinson, D.P., Justh, H.L., Kass, D.M. Lewis, S.R., Mischna, M.A., Murphy, J.R., Rafkin, S.C.R., Tyler, D., Withers, P.G., 2012. Assessment of environments for Mars Science Laboratory entry, descent and surface operations. Space Sci Rev, doi: 10.1007/s11214-012-9911-3